ACS OMEGA

http://pubs.acs.org/journal/acsodf

Article

Synthesis and Characterization of Cobalt-Doped Ferrites for Biomedical Applications

Muhammad Naeem Kiani, Muhammad Shoaib Butt,* Iftikhar Hussain Gul, Mohsin Saleem, Muhammad Irfan, Abrar H. Baluch, Muhammad Aftab Akram, and Mohsin Ali Raza

Cite This: *ACS Omega* 2023, 8, 3755−3761

Read Online

ACCESS | Metrics & More | Article Recommendations

ABSTRACT: Novel materials for biomedical applications are in critical need of time. In the present work, the antibacterial properties of $Co_{1-x}Ni_xMg_xFe_2O_4$ nanoparticles (NPs) are assessed by the disc diffusion method for the common pathogen, that is, Gram-negative (*Escherichia coli* and *Pseudomonas aeruginosa*) and Gram-positive (*Staphylococcus aureus*) bacteria. Overnight grown bacterial cultures were individually lawn-cultured on nutrient agar plates. All samples of NP concentrations (2 mg/mL) were prepared in sterile water and dispensed by sonication. Sterile filter paper discs (1.0 mm) were saturated by the (doped $CoFe_2O_4$) NP solution and incubated at 37 ± 0.1 °C for 24 h. The NPs with a fine size of 30−70 nm of $Co_{1-x}Ni_xMg_xFe_2O_4$ were achieved using the sol−gel method by doping $CoFe_2O_4$ initially with Ni and codoping with Mg, and their properties were studied by X-ray diffraction, scanning electron microscopy, energy-dispersive X-ray spectroscopy, and Fourier transform infrared techniques. According to the results, $Co_{0.5}Ni_{0.25}Mg_{0.25}Fe_2O_4$ NPs exhibited potent antibacterial activities against *s. aureus* having an inhibition zone of 6.5 mm and *P. aeruginosa* having an inhibition zone of 6 mm as that were examined. The result shows that the bacteriostatic properties of NPs are used for numerous applications such as hyperthermia, antibacterial treatments, and targeted drug delivery.

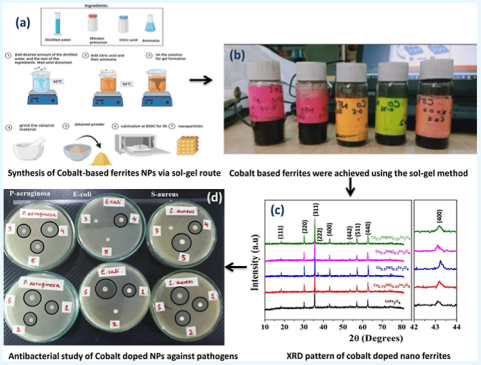

1. INTRODUCTION

Recently, magnetic nanoparticles (NPs) have attracted substantial consideration in the field of biomedical because of their beneficial magnetic, optical, and antibacterial features at the nanoscale. The magnetic nanoferrites are generally represented as MFe_2O_4 where M represents either Ni, Co, or Cu which are tetrahedral sites of typical bivalent cations in a cubic lattice structure.[1] Co is used as a source of gamma rays for sterilizing medical equipment and consumer products, radiation therapy for treating cancer patients, and for manufacturing plastics.[2] Furthermore, Co is used for food irradiation; depending on the radiation dose, the irradiating process is used to sterilize food, destroy pathogens, extend the shelf-life of food, disinfest fruits and grain, delay ripening, and retard sprouting like potatoes and onions. Cobalt ferrite, $CoFe_2O_4$ (CFO), a ferrimagnet having inverse spinel, is one of the most commercially significant members of the magnetic ferrite class.[3] The spinel structure in cobalt ferrite is inverse and has various advantages due to its good coupling efficiency, high magnetostrictiveness, and low cost among other different spinel ferrites.[4,5] $CoFe_2O_4$ has attracted special attention on account of its unique physical features, including high Curie temperature, large magnetocrystalline anisotropy, high coercivity, excellent chemical stability, large magnetostrictive coefficient, mechanical hardness, and moderate saturation magnetization. Magnetic properties are greatly dependent upon its crystal orientation; it shows excellent electrical insulation.[6,7] Furthermore, from previous studies, it was confirmed that $CoFe_2O_4$ is a magnetic particle and there is an increase in magnetic properties by increasing the Mg and Ni concentrations.[8,9]

Metal ferrite NPs indicate substantial antibacterial activities.[10] Transition-metal-substituted cobalt ferrite NPs have the most effective contact biocidal property among all of the NPs.[11] Among these metal ferrite NPs, cobalt ferrite NPs show high biocompatibility, and their antibacterial activity makes them an appropriate option for antibacterial uses in the industrial, food, and medical fields.[12−14] $CoFe_2O_4$ plays a major role in medical applications and the chemical industry like biosensors and gas sensors.[15] In the biomedical field, cobalt ferrite NPs are utilized for applications such as computer tomography (CT scan), contrast agents of magnetic resonance imaging, and tumor treatment viz. targeted drug

Received: August 15, 2022
Accepted: November 28, 2022
Published: January 18, 2023

https://doi.org/10.1021/acsomega.2c05226
ACS Omega 2023, 8, 3755−3761

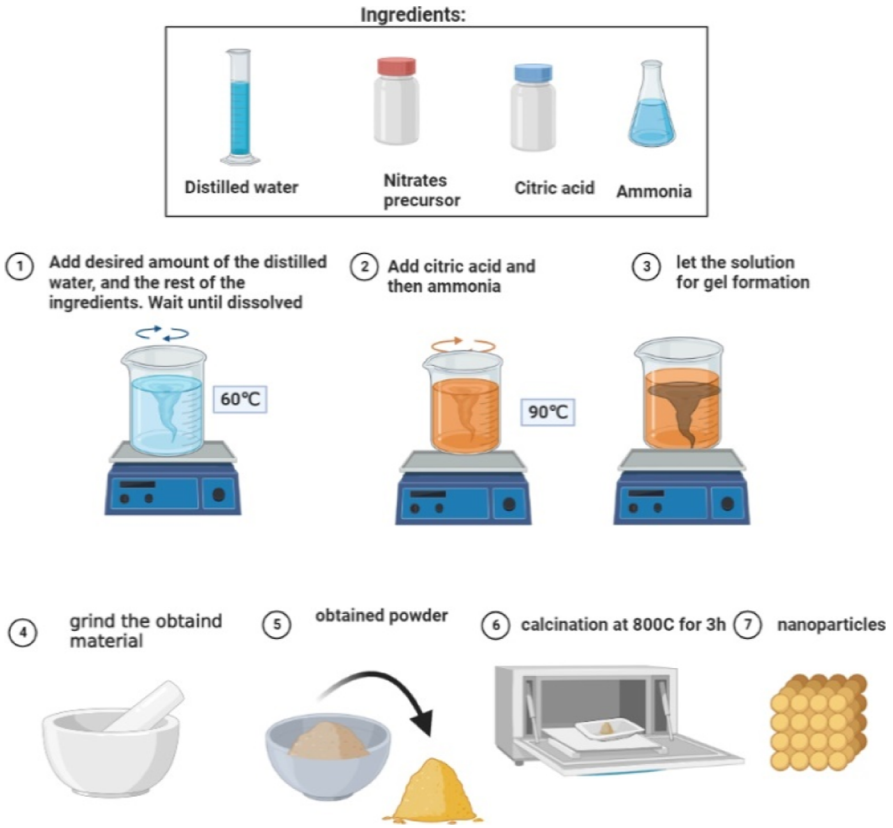

Figure 1. Synthesis of cobalt-based ferrite NPs via the sol−gel route.

delivery and hyperthermia.[16,17] These are the essential factors that influence biomedical applications. The effectiveness of these NPs is biocompatibility and easy surface functionalization.[18] Yamamoto et al. reported the influence of particle size on the antibacterial activity and reported that the activity increased with decreasing particle size.[19] The antimicrobial application of magnetic NPs is gaining attention because they can be manipulated through an external magnetic field. Moreover, many nonmagnetic metal NPs or metal oxides were found to be antimicrobials against pathogenic bacteria. Gole et al. reported the antibacterial study of cobalt ferrites by agar well diffusion method and found positive results against the most common pathogen such as *Escherichia coli*.[20] Velho-Pereira et al. reported that cobalt ferrite NP systems have antibacterial activity against multidrug-resistant clinical pathogens, namely, Gram-positive bacteria *Staphylococcus epidermidis* and Gram-negative bacteria *E. coli*.[21] Nickel ferrite ($NiFe_20_4$) NPs have excellent antibacterial properties against *S. aureus* and *Pseudomonas aeruginosa*, making them a good source of disinfectant in polluted water bodies with powerful properties that improve microbe inhibition.[22,23] Recent studies showed that the nickel nanoferrites are well known for having unique properties such as high permeability under high-frequency conditions and electrical resistivity in magnetic data storage devices, radar and microwave devices, biomedical fields, and nanoscale electronic systems.[24] Due to their capacity to show surface disorderliness, nickel ferrite, a member of the group of cubic ferromagnetic oxides, can exhibit this exceptional property.

The ferrimagnetic substance cobalt−nickel (Co−Ni) ferrite has the highest magnetocrystalline anisotropy and magnetostriction coefficient among ferrites. It is well-known that Co and Ni are both inverse spinel with homogeneous distribution in the A and B lattice sites. As a result, their magnetic properties are attributed to the antiferromagnetic coupling between the tetrahedral and octahedral sublattices. Additionally, nickel-substituted cobalt ferrites exhibit good chemical stability and are used as a binder and magnetic filler in nanocomposites for electromagnetic shielding. Furthermore, it is generally expected that rare-earth-substituted spinel ferrites will often exhibit superior electric and magnetic characteristics when compared to their counterparts made of pure spinel.[25]

An appropriately designed hybrid system of alumina-based nickel ferrite would be beneficial for potential use as an antimicrobial or drug delivery agent to specific organs in the human body system, considering the accessibility, suitability, and widespread application of alumina in various applications. Sanpo et al.[29] suggested a new approach to enhancing the antibacterial activity of ferrite NPs for biomedical applications by substituting the transition metal with the spinel ferrite.[26] The objective of this research work is to investigate the effect of doping of Mg and Ni in cobalt ferrite NPs with different concentrations of $Co_{0.75}Ni_{0.5}Fe_2O_4$, $Co_{0.5}Ni_{0.5}Fe_2O_4$, $Co_{0.5}Mg_{0.5}Fe_2O_4$, and $Co_{0.5}Ni_{0.25}Mg_{0.25}Fe_2O_4$, and from disc diffusion method, it was confirmed that codoping with Ni and Mg concentration shows antibacterial properties.

2. MATERIAL DETAILS

The raw materials used in this work were the salts of iron nitrate (nano hydrated [$Fe\ (NO_3)_2{\cdot}9H_2O$]), magnesium nitrate (hexa-hydrated [$Mg(NO_3)_2$]), cobalt nitrate (hexa-hydrated [$Co(NO_3)_2{\cdot}(H_2O)_6$]), nickel nitrate (hexa-hydrated [$Ni(NO_3)_2{\cdot}6H_2O$]), citric acid (CA) [$C_6H_8O_7$], deionized

https://doi.org/10.1021/acsomega.2c05226
ACS Omega 2023, 8, 3755−3761

water, and ammonia [NH_4OH] which were procured from Merck & Co.

2.1. Synthesis of NPs. The remarkable structural, electrical, and magnetic properties of ferrites, a large class of magnetic oxides, make them suitable for a wide range of applications. These characteristics are highly influenced by the preparation technique. The sol−gel method has many advantages over other techniques for producing ferrite with the desired nanoarchitecture.[27]

The sol−gel method was used to synthesize the cobalt-doped ferrites.[28] The specific amounts of dehydrating iron(III) nitrate, cobalt nitrate, nickel nitrate, and magnesium nitrate were added to the solution, DI water was used as a solvent and to make the product. The solution was kept on a hot plate at 60−90 °C temperature. After 15 to 20 min of continuous stirring, ammonia was added to maintain the pH of the solution. CA was used as a fuel, keeping metal nitrates to CA molar ratio 1:2.[29] After that, the final solution was set at 120 °C to allow gel formation. In the later stage, the gel automatically ignited and burnt with high-temperature glowing flints.[30] The gels were dried and ground to obtain nanoferrite powders. The powders were annealed at 800 °C for 3 h in a muffle furnace to obtain desired degrees of crystallinity. The illustration synthesis process has been made with BioRender software, as shown in Figure 1 and the schematic diagram in Figure 2, respectively.

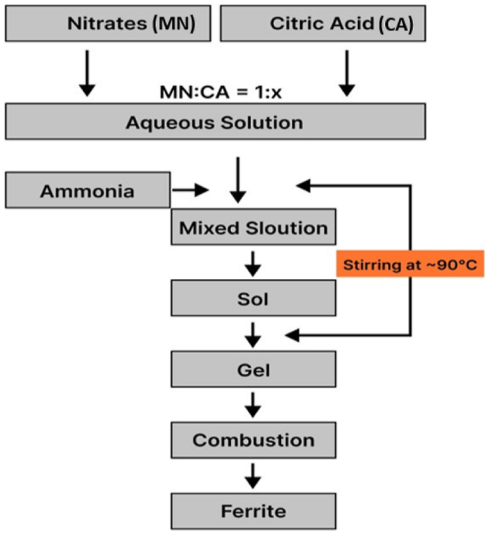

Figure 2. Schematic flow sheet for the preparation of NPs.

3. RESULTS AND DISCUSSION

3.1. XRD Analysis. The X-ray diffraction (XRD) patterns of all synthesized samples in the 2θ range of 20−80° are shown in Figure 3.

The XRD patterns were indexed and confirmed, and the peaks were well-matched with JCPDS no. (00-003-0864). The diffraction peaks of synthesized NPs corresponded to the (111), (220), (311), (222), (400), (422), (511), and (440) planes, confirming that the structure of synthesized NPs was single-phase. The lattice constant and unit cell volume of the samples were found to be decreased with the increase of Mg contents, which was due to the substitution of relatively smaller Mg^{+2} (0.72 Å) ions for larger Co^{+2} (0.74 Å) ions. The effect of Ni substitution was also seen that the results showed a ferrite

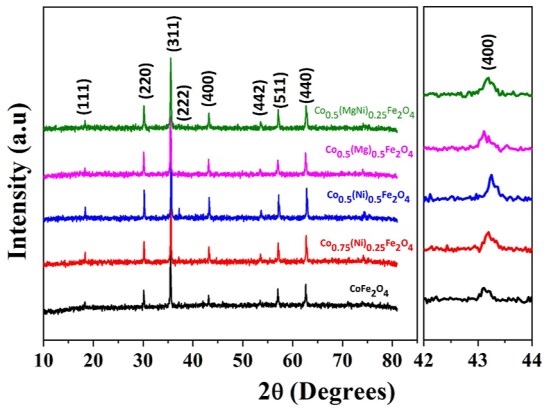

Figure 3. XRD pattern of cobalt-doped nanoferrites.

structure of cubic lattice, and the lattice constant decreased with an increase of the Ni content. This is due to the smaller ionic radius of nickel ions (0.63 Å) replacing the cobalt ion (0.78 Å) site.[31] The lattice constant has been calculated by using eq 1.

$$\frac{1}{d^2} = \frac{h^2 + k^2 + l^2}{a^2} \quad (1)$$

where d is the interplanar spacing, (h k l) is the miler indices, and (a) is the lattice constant. The crystallite size is also calculated using Scherrer's formula, as shown in eq 2.[32]

$$t = \frac{k\lambda}{\beta \cos \theta} \quad (2)$$

where β is the full width peak at half-maximum (in radians) at the observed peak angle 2θ, k is the crystallite shape factor (and was considered as 0.94), and λ is the wavelength of X-ray. The comparison of Mg-substituted and Ni-substituted cobalt ferrites is summarized in Table 1.

Table 1. XRD Comparison Table of $CoFe_2O_4$ with Ni- and Mg-Doped $CoFe_2O_4$ NPs

sample compositions	peak position	lattice parameter (Å)	crystallite size (nm)
$CoFe_2O_4$	35.85	8.3846	48.08
$Co_{0.75}Ni_{0.25}Fe_2O_4$	35.72	8.3685	42.48
$Co_{0.5}Ni_{0.5}Fe_2O_4$	35.64	8.3421	29.47
$Co_{0.5}Mg_{0.5}Fe_2O_4$	35.49	8.3367	30.56
$Co_{0.5}Ni_{0.25}Mg_{0.25}Fe_2O_4$	35.43	8.3764	44.45

The average crystallite size is calculated to be 48.08 nm for the undoped samples, and the crystallite sizes of the doped samples have been calculated to give an average size of 29−49 nm by using the dominant peak (311). Ni-doped cobalt ferrites have a minimum crystallite size of 29.47 nm for x = 0.5 concentration. Also, the lattice parameter varies from 8.3846 to 8.3367 Å with its maximum and minimum values of 8.3846 Å for x = 0.5 Ni-doped and 8.3367 Å for x = 0.5 Mg-doped, respectively.

3.2. EDX Analysis. The energy-dispersive X-ray (EDX) spectral analysis of the synthesized $CoFe_2O_4$ and CoNiMgFe$_2$O$_4$ is illustrated in Figure 4a,b, respectively. The ratio of EDX peaks represents the expected elemental composition of synthesized NPs. The synthesized product contains Co, Fe, and O, as shown in Figure 4a, and Co, Ni, Mg, Fe, and O as

https://doi.org/10.1021/acsomega.2c05226
ACS Omega 2023, 8, 3755−3761

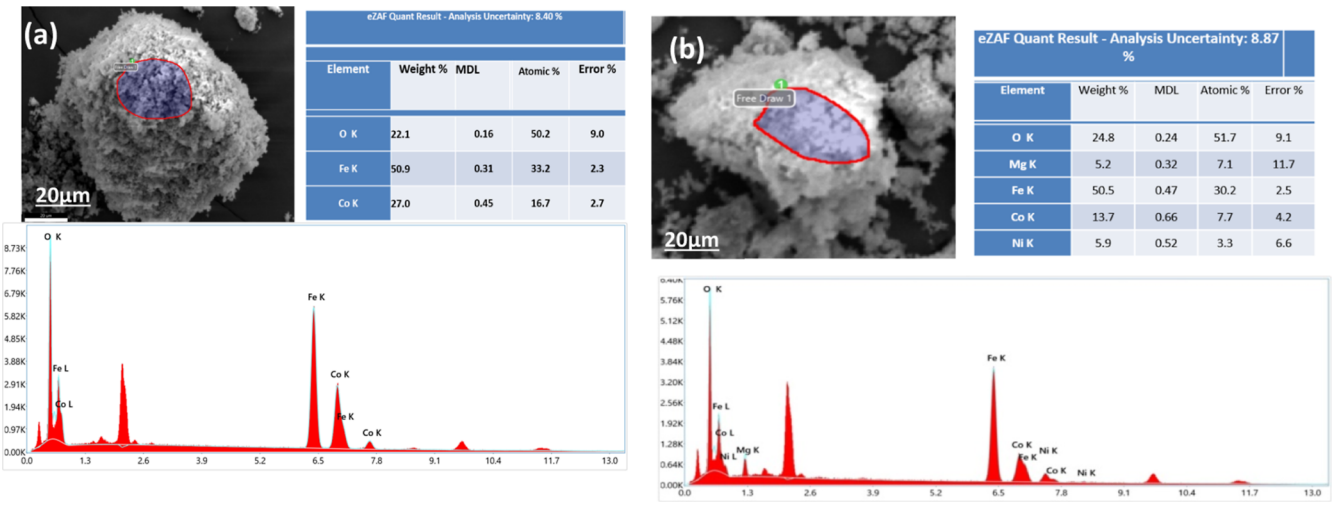

Figure 4. EDX results of (a) $CoFe_2O_4$ and (b) $CoNiMgFe_2O_4$.

well. Thus, it indicates that the achieved NPs do not contain any other impurities.

3.3. FTIR Analysis. Fourier transform infrared (FTIR) spectra are frequently used to investigate the structure of a multicomponent system. Our synthesized samples' FTIR spectra were observed at room temperature (25−27 °C) which supported the formation of the spinel structure and its cationic distribution. The FTIR spectra of all the doped cobalt ferrite NP samples, measured in the wave number range of 250−1000 cm^{-1}, are shown in Figure 5. The presence of two typical peaks in the FTIR spectra of all the compositions specifies the formation of the spinel phase in all samples.

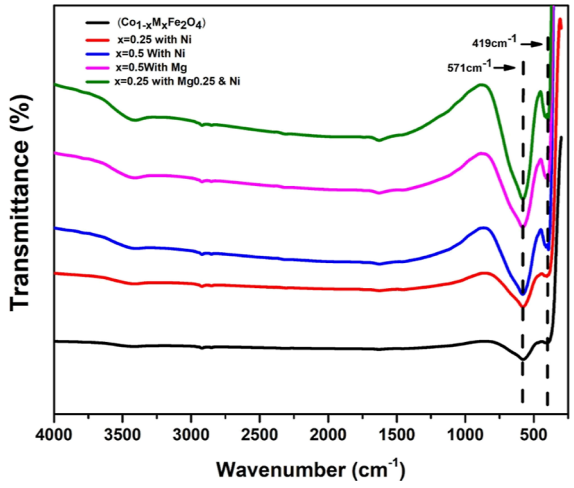

Figure 5. FTIR spectra of cobalt-doped nanoferrites.

The intense peak at 419 cm^{-1} is attributed to stretching vibrations of octahedral site complexes (metal cation and oxygen), whereas the peak at around 571 cm^{-1} is attributed to tetrahedral complexes.

3.4. SEM Analysis. The scanning electron microscopy (SEM) images show the surface morphology of the synthesized cobalt ferrite magnetic NPs which are shown in Figure 6.

The size of the NPs is roughly spherical (cubic) and distributed throughout the sample. The average particle size determined from SEM images is noted as 29−49 nm, which is closer to the size determined from XRD data.

In Figure 6b, Ni- and Mg-doped cobalt ferrite NPs agglomerated due to less time of sonication that results in poor particle separation moreover due to their magnetic properties and the binding of primary particles held together by weak surface interactions such as the van der Waals force. Irregular morphology (with no regular particle shapes) and agglomeration of the particles seem to be a signature of the gel formation after heating the solution, which is also observed in the calcined samples.

3.5. Antibacterial Activity. The disc diffusion method was used to determine the activity of the prepared samples ($CoFe_2O_4$, $Co_{0.75}Ni_{0.5}Fe_2O_4$, $Co_{0.5}Ni_{0.5}Fe_2O_4$, $Co_{0.5}Mg_{0.5}Fe_2O_4$, and $Co_{0.5}Ni_{0.25}Mg_{0.25}Fe_2O_4$). All above-mentioned samples were characterized against the Gram-negative (*P. aeruginosa* and *E. coli*) and Gram-positive (*S. aureus*) bacteria. The pathogenic bacteria were obtained from the Atta-Ur-Rehman School of Applied Biosciences (ASAB), National University of Science and Technology (NUST), H-12, Islamabad. The bacterium was selected based on the widespread infection that it caused when it was present in contaminated water and spread throughout the community. For instance, *E. coli* causes vomiting and diarrhea, while *P. aeruginosa*, a very pathogenic microbe, causes whooping cough in both children and adults. In the meantime, *S. aureus* has an impact, is a contributing bacterium in boils, and complicates wounds. Overnight-grown bacterial cultures were individually lawn-cultured on nutrient agar plates. All samples of concentration 2 mg/mL were prepared in sterile water and dispensed by sonication. Sterile filter paper discs (1.0 mm) were saturated by the undoped $CoFe_2O_4$ and Mg- and Ni-doped $CoFe_2O_4$ NP solution and placed above the culture and incubated at 37 ± 0.1 °C for 24 h after which the zone of inhibition was recorded. The ceftriaxone (CRO) antibacterial was used as a control. The same concentrations for bacterial linear growth were examined, whereas each concentration was individually set in Petri dishes. The schematic diagram is shown in Figure 7.

The antibacterial test of cobalt-doped ferrite NPs against the Gram-negative (*P. aeruginosa* and *E. coli*) and Gram-positive (*S. aureus*) bacteria was carried out, as shown in Figure 8, and Table 2 shows sample IDs for investigating antibacterial study.

The result shows that antibiotic ciprofloxacin was used as a reference/standard to compare antibacterial activities. The

https://doi.org/10.1021/acsomega.2c05226
ACS Omega 2023, 8, 3755−3761

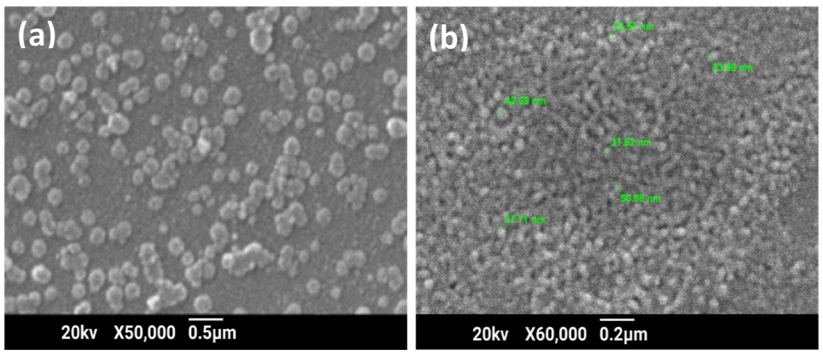

Figure 6. SEM images (a) $CoFe_2O_4$ and (b) $CoNiMgFe_2O_4$.

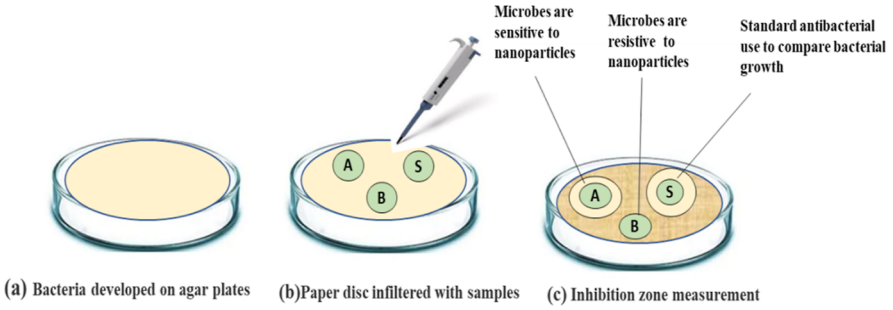

Figure 7. Disc diffusion method: (a) bacteria developed on agar plates, (b) paper disc infiltered with samples, and (c) inhibition zone measurement.

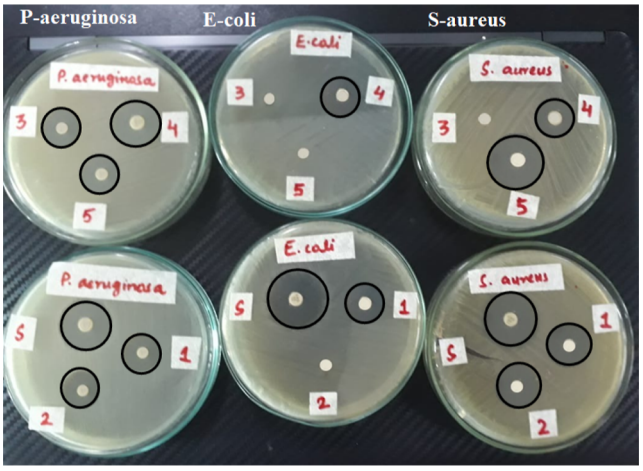

Figure 8. Antibacterial study of cobalt-doped NPs against pathogens.

Table 2. Sample IDs for Investigating Antibacterial Study, as Shown in Figure 8

sample IDs	abbreviates
CRO	standard S
$CoFe_2O_4$	S1
$Co_{0.75}Ni_{0.5}Fe_2O_4$	S2
$Co_{0.5}Ni_{0.5}Fe_2O_4$	S3
$Co_{0.5}Mg_{0.5}Fe_2O_4$	S4
$Co_{0.5}Ni_{0.25}Mg_{0.25}Fe_2O_4$	S5

synthesized compounds were dissolved in sterile water, and each stock solution is 2 mg/mL in concentration. The seeded plates were incubated at 37 °C for 24 h. The diameter of inhibition zones was measured, and the percentage inhibition of test compounds was related to the standard drug whose zone of inhibition was taken as 100%. The results of the minimum inhibitory zone of the synthesized compounds against bacterial species are determined, that is, the standard has 8 mm zone, while the synthesized NPs showed different results. The graphical representation of the activity is shown in Figure 9. These results revealed that ($CoFe_2O_4$) NPs efficiently

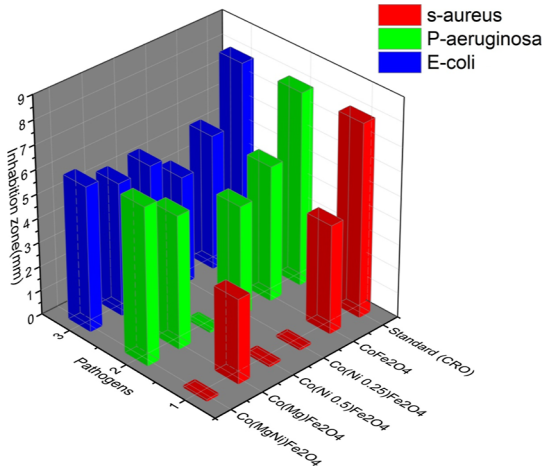

Figure 9. Graphical representations of the zone of inhibition (mm) of all cobalt ferrites against *S. aureus*, *E. coli*, and *P. aeruginosa*.

inhibited the growth of the microbes, and $CoFe_2O_4$ NPs showed potential antimicrobial activity against *P. aeruginosa*, *S. aureus*, and *E. coli*.

3.5.1. Inhibition Zone. The standard CRO zone was investigated after 24 h incubation and was measured using a micrometer of about 8 mm. In the case of *P. aeruginosa*, $CoFe_2O_4$ inhibition zone was around 5.6 mm which is close to that of the standard. $CoFe_2O_4$ doped with Ni (x = 0.25 and

https://doi.org/10.1021/acsomega.2c05226
ACS Omega 2023, 8, 3755−3761

0.5) has 4.5 and 5.6 mm zones, respectively. Furthermore, $CoFe_2O_4$ doped with Mg (x = 0.5) has 5.5 mm zone, and $CoFe_2O_4$ doped with Mg and Ni (x = 0.25) has 6 mm zone which shows that there is an increase in the inhibition zone. In the case of *E. coli*, $CoFe_2O_4$ doped with Ni (x = 0.25) and codoped with Ni and Mg (x = 0.25) shows no response to pathogens. On the other hand, the inhibition zone of undoped $CoFe_2O_4$ and that doped with Mg (x = 0.5) was measured at about 4.5 mm, respectively. In the case of *S. aureus*, $CoFe_2O_4$ has an inhibition zone to the standard (CRO) of 5.6 mm and $CoFe_2O_4$ doped with Ni (x = 0.25 and 0.5) has 4.6 and 5.6 mm zones, respectively. Furthermore, $CoFe_2O_4$ doped with Mg (x = 0.5) has 5.4 mm zone, and $CoFe_2O_4$ doped with Mg and Ni (x = 0.25) has 6.5 mm zone which is closer to the standard (CRO) and there is an increase in the inhibition zone. Therefore, our final sample is active against *S. aureus* and *P. aeruginosa*.

These results revealed that cobalt-doped ferrite NPs efficiently inhibited the growth of the microbes. However, the concentration of Mg has a minimum effect against *E. coli*.

4. CONCLUSIONS

Cobalt ferrite NPs doped with Ni and Mg have been successfully synthesized by the sol−gel method that employs CA as a capping agent. Metals doped with cobalt ferrite NPs formed a cubic spinel structure and exhibit irregular morphology with crystallite size varying from 29 to 49 nm. The spinel structure of cobalt ferrite NPs is confirmed by FTIR which shows the two main broad metal oxygen bands (419 and 571 cm^{-1}). From SEM analysis, the particles are spherical, with some clustering and agglomeration between the particles. The EDX spectra show the presence of Co, Fe, and O in $CoFe_2O_4$ and Co, Ni, Mg, Fe, and O in $Co_{1-x}Ni_xMg_xFe_2O_4$ as well. The doping of Mg and Ni in cobalt ferrite NPs significantly improved antibacterial activities against *S. aureus* and *P. aeruginosa*. The antibacterial activity of $Co_{1-x}Ni_xMg_xFe_2O_4$ NPs against *S. aureus* is higher than that against *P. aeruginosa* and *E. coli*. The bactericidal studies show that $Co_{1-x}Ni_xMg_xFe_2O_4$ can be a major part of biomedical sensing drug delivery and kill cancer cells as an anticancer drug carrier.

AUTHOR INFORMATION

Corresponding Author

Muhammad Shoaib Butt − *School of Chemical and Material Engineering (SCME), National University of Science and Technology (NUST), Islamabad 44000, Pakistan;* orcid.org/0000-0002-7689-339X; Email: muhammad.shoaib@scme.nust.edu.pk

Authors

Muhammad Naeem Kiani − *School of Chemical and Material Engineering (SCME), National University of Science and Technology (NUST), Islamabad 44000, Pakistan*

Iftikhar Hussain Gul − *School of Chemical and Material Engineering (SCME), National University of Science and Technology (NUST), Islamabad 44000, Pakistan*

Mohsin Saleem − *School of Chemical and Material Engineering (SCME), National University of Science and Technology (NUST), Islamabad 44000, Pakistan*

Muhammad Irfan − *School of Chemical and Material Engineering (SCME), National University of Science and Technology (NUST), Islamabad 44000, Pakistan*

Abrar H. Baluch − *Department of Materials Science and Engineering, Institute of Space Technology, Islamabad 44000, Pakistan;* orcid.org/0000-0003-2385-8328

Muhammad Aftab Akram − *Department of Materials Science & Engineering, Pak-Austria Fachhochschule, Institute of Applied Sciences & Technology, Haripur 22650, Pakistan*

Mohsin Ali Raza − *Institutes of Metallurgy and Materials Engineering, University of the Punjab, Lahore 54590, Pakistan*

Complete contact information is available at: https://pubs.acs.org/10.1021/acsomega.2c05226

Notes

The authors declare no competing financial interest.

ACKNOWLEDGMENTS

This work was acknowledged, with pleasure, with support from the Pakistan Science Foundation (PSF) G-5/2, Islamabad-Pakistan, with a PSF grant (PSF/Res/C-NUST/Med 521).

REFERENCES

(1) Nigam, A.; Pawar, S. J. Structural, magnetic, and antimicrobial properties of zinc doped magnesium ferrite for drug delivery applications. *Ceram. Int.* **2020**, *46*, 4058−4064.

(2) Ishaq, K.; et al. Characterization and antibacterial activity of nickel ferrite doped α-alumina nanoparticle. *Eng. Sci. Technol. an Int. J.* **2017**, *20*, 563−569.

(3) Shirsath, S. E.; Liu, X.; Yasukawa, Y.; Li, S.; Morisako, A. Switching of magnetic easy-axis using crystal orientation for large perpendicular coercivity in CoFe2O4 thin film. *Sci. Rep.* **2016**, *6*, 30074.

(4) Aghrich, K.; et al. Experimental and first-principles study of the origin of the magnetic properties of CoFe2O4 spinel ferrite. *Appl. Phys. A: Mater. Sci. Process.* **2020**, *126*, 940.

(5) Ahmad, Z.; et al. Structural and complex impedance spectroscopic studies of Mg-substituted CoFe2O4. *Ceram. Int.* **2016**, *42*, 18271−18282.

(6) Amiri, S.; Shokrollahi, H. The role of cobalt ferrite magnetic nanoparticles in medical science. *Mater. Sci. Eng. C* **2013**, *33*, 1−8.

(7) Munawar, T.; et al. Synthesis, characterization, and antibacterial study of novel Mg0.9Cr0.05M0.05O (M = Co, Ag, Ni) nanocrystals. *Phys. B Condens. Matter* **2021**, *602*, 412555.

(8) Mund, H. S.; Ahuja, B. L. Structural and magnetic properties of Mg doped cobalt ferrite nano particles prepared by sol-gel method. *Mater. Res. Bull.* **2017**, *85*, 228−233.

(9) Velhal, N. B.; Patil, N. D.; Shelke, A. R.; Deshpande, N. G.; Puri, V. R. Structural, dielectric and magnetic properties of nickel substituted cobalt ferrite nanoparticles: Effect of nickel concentration. *AIP Adv.* **2015**, *5*, 097166.

(10) Bose, S.; Banerjee, M. Magnetic particle capture for biomagnetic fluid flow in stenosed aortic bifurcation considering particle-fluid coupling. *J. Magn. Magn. Mater.* **2015**, *385*, 32−46.

(11) Phugate, D. V.; et al. Effect of Ho3+ Ion Doping on Thermal, Structural, and Morphological Properties of Co−Ni Ferrite Synthesized by Sol-Gel Method. *J. Supercond. Nov. Magnetism* **2020**, *33*, 3545−3554.

(12) Li, Z.; Aik Khor, K. Preparation and properties of coatings and thin films on metal implants. *Encycl. Biomed. Eng.* **2019**, *13*, 203−212.

(13) Kumar, P.; Mahajan, P.; Kaur, R.; Gautam, S. Nanotechnology and its challenges in the food sector: a review. *Mater. Today Chem.* **2020**, *17*, 100332.

(14) Gheidari, D.; Mehrdad, M.; Maleki, S.; Hosseini, S. Synthesis and potent antimicrobial activity of CoFe2O4 nanoparticles under visible light. *Heliyon* **2020**, *6*, No. e05058.

(15) Paul, J.; Philip, J. Inter-digital capacitive ethanol sensor coated with cobalt ferrite nano composite as gas sensing material. *Mater. Today Proc.* **2020**, *25*, 148−150.
(16) Jun, Y. W.; Seo, J. W.; Cheon, J. Nanoscaling laws of magnetic nanoparticles and their applicabilities in biomedical sciences. *Acc. Chem. Res.* **2008**, *41*, 179−189.
(17) Virlan, C.; Bulai, G.; Caltun, O.; Hempelmann, R.; Pui, A. Rare earth metals' in fl on the heat generating capability of cobalt ferrite nanoparticles. *Ceram. Int.* **2016**, *42*, 11958−11965.
(18) Sharifianjazi, F.; et al. Magnetic CoFe2O4 nanoparticles doped with metal ions: A review. *Ceram. Int.* **2020**, *46*, 18391−18412.
(19) Yamamoto, O. Influence of particle size on the antibacterial activity of zinc oxide. *Int. J. Inorg. Mater.* **2001**, *3* (7), 643−646.
(20) Gole, D. A.; Kapatkar, S. B.; Mathad, S. N.; Chavan, R. R. IN VITRO ANTIMICROBIAL ACTIVITY OF COBALT FERRITE NANOPARTICLES SYNTHESIZED BY Co-PRECIPITATION METHOD. *Acta Chem. Iasi* **2020**, *28*, 225−236.
(21) Velho-Pereira, S.; et al. Antibacterial action of doped CoFe2O4 nanocrystals on multidrug resistant bacterial strains. *Mater. Sci. Eng. C* **2015**, *52*, 282−287.
(22) Iqbal, S.; et al. Structural, morphological, antimicrobial, and in vitro photodynamic therapeutic assessments of novel Zn+2-substituted cobalt ferrite nanoparticles. *Results Phys.* **2019**, *15*, 102529.
(23) Mahmoodpour, M.; Goharkhah, M.; Ashjaee, M. Investigation on trajectories and capture of magnetic drug carrier nanoparticles after injection into a direct vessel. *J. Magn. Magn. Mater.* **2020**, *497*, 166065.
(24) Selmi, A.; et al. Synthesis, structural and complex impedance spectroscopy studies of Ni0.4Co0.4Mg0.2Fe2O4 spinel ferrite. *Phase Transitions* **2017**, *90*, 942−954.
(25) Almessiere, M. A.; et al. Impact of Tm3+ and Tb3+ rare earth cations substitution on the structure and magnetic parameters of Co-Ni nanospinel ferrite. *Nanomaterials* **2020**, *10*, 2384.
(26) Sanpo, N.; Berndt, C. C.; Wen, C.; Wang, J. Transition metal-substituted cobalt ferrite nanoparticles for biomedical applications. *Acta Biomater.* **2013**, *9* (3), 5830−5837.
(27) Shirsath, S. E.; Wang, D.; Jadhav, S. S.; Mane, M. L.; Li, S.Ferrites Obtained by Sol-Gel Method. In *Handbook of Sol-Gel Science and Technology: Processing, Characterization and Applications*; Klein, L., Aparicio, M., Jitianu, A., Eds.; Springer International Publishing, 2018; pp 695−735.
(28) Shirsath, S. E.; Wang, D.; Jadhav, S.; Mane, M. L.*Handbook of Sol-Gel Science and Technology*; Handbook of Sol-Gel Science and Technology, 2017.
(29) Sanpo, N.; Berndt, C. C.; Wen, C.; Wang, J. Transition metal-substituted cobalt ferrite nanoparticles for biomedical applications. *Acta Biomater.* **2013**, *9*, 5830−5837.
(30) Shirsath, S. E.; Wang, D.; Jadhav, S. S.; Mane, M. L.; Li, S.Ferrites obtained by sol-gel method. *Handbook of sol-gel science and technology*; Springer Cham, 2018; Vol. *695*−*735*.
(31) Revathi, J.; et al. Synthesis and characterization of CoFe2O4 and Ni-doped CoFe2O4 nanoparticles by chemical Co-precipitation technique for photo-degradation of organic dyestuffs under direct sunlight. *Phys. B Condens. Matter* **2020**, *587*, 412136.
(32) Bhandare, S. V.; et al. Effect of Mg-substitution in Co−Ni-Ferrites: Cation distribution and magnetic properties. *Mater. Chem. Phys.* **2020**, *251*, 123081.

https://doi.org/10.1021/acsomega.2c05226
ACS Omega 2023, 8, 3755−3761